Hydrodynamic Effect on the Inhibition for the Flow Accelerated Corrosion of an Elbow

L. Zeng, G. A. Zhang[†], and X. P. Guo

School of Chemistry and Chemical Engineering, Huazhong University of Science and Technology, Wuhan 430074, P.R. China

The inhibition effect of thioureido imidazoline inhibitor (TAI) for flow accelerated corrosion (FAC) at different locations for an X65 carbon steel elbow was studied by array electrode and computational fluid dynamics (CFD) simulations. The distribution of the inhibition efficiency measured by electrochemical impedance spectroscopy (EIS) is in good accordance with the distribution of the hydrodynamic parameters at the elbow. The inhibition efficiencies at the outer wall are higher than those at the inner wall meaning that the lower inhibition efficiency is associated with a higher flow velocity, shear stress, and turbulent kinetic energy at the inner wall of the elbow, as well as secondary flow at the elbow rather than the mass transport of inhibitor molecules. Compared to the static condition, the inhibition efficiency of TAI for FAC was relatively low. It is also due to a drastic turbulence flow and high wall shear stress during the FAC test, which prevents the adsorption of inhibitor and/or damages the adsorbed inhibitor film.

1. Introduction

Flow accelerated corrosion (FAC), which usually results in the failure of pipelines, is an important and inevitable challenge in the oil and gas industry [1,2]. The use of carbon steel associated with chemical inhibitors treatment remains the most common method for corrosion control [3-5]. Nitrogen-based organic compounds, such as imidazolines or their derivatives, have been used successfully as corrosion inhibitors in the oil and gas industries [6,7]. Since the fluid hydrodynamics affect the mass transfer process of corrosion reactions and the adsorption of inhibitors on the steel surface, the fluid flow has substantial influence on the inhibition effect of inhibitors. Therefore, it is necessary to reveal the effect of hydrodynamics on the inhibition performance of inhibitors for FAC.

In the oil and gas transportation, elbow is an important part of most practical pipe configurations. However, the flow regime in a 90° elbow is subject to great changes in flow direction and flow velocity [8]. Therefore, it is expected that there would be significant difference in the inhibition effect of inhibitors at different locations of the elbow. Array electrode can be used for determining the inhibition effect difference at different locations of the elbow.

In this work, the inhibition effect difference of thioureido imidazoline inhibitor (TAI) for the FAC at different locations of X65 carbon steel elbow was studied by electrochemical measurements and surface characterization with placing array electrodes at different locations of the elbow. Computational fluid dynamics (CFD) simulation was also performed to reveal the flow regime within the pipeline elbow, and to determine the correlation between the inhibition efficiency of TAI and the hydrodynamics at different locations of the elbow.

2. Experimental and CFD Simulation

To study the inhibition effect of TAI for the FAC at the elbow, array electrodes (X65 pipeline steel with each exposed area of 0.3 cm^2) were used. Before FAC test, array electrodes surface were abraded with 800 grit silicon carbide paper, rinsed with deionized water, degreased with acetone and air-dried.

The testing solution, containing 90.44 g/L NaCl, 2.20 g/L KCl, 0.43 g/L CaCl$_2$, 0.43 g/L Na$_2$SO$_4$, 6.33 g/L MgCl2.6H$_2$O, 0.49 g/L NaHCO$_3$, was prepared from analytical reagents and deionized water to simulate the formation water of an oil field. Prior to FAC test, the solution

---

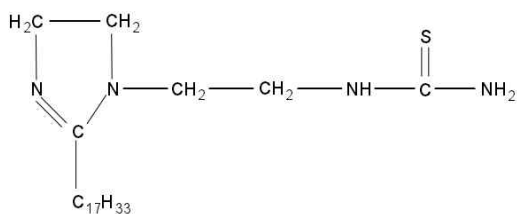[†] Corresponding author: zhangguoan@gmail.com

Fig. 1 Chemical structure of thioureido imidazoline inhibitor.

was deaerated by purging CO_2 gas (purity was 99.95%) for 12 h. After deaeration, inhibitor was injected to the solution. An imidazoline derivative inhibitor (TAI), as shown in Fig. 1, was used in this study.

A circulating loop system was used for FAC test, as shown in Fig. 2a. It consisted of pipes, a centrifugal pump, a reservoir, a pressure gage, a flow meter and test section. After pretreatment, array electrodes were mounted into test section with the same spacing distance in flow direction. Fig. 2c shows the assembly of elbow test section, with 21 specimens at the outer wall of the elbow, and 9 specimens at the inner wall. The exposed surface

of each electrode was in accordance with the internal surface of pipeline, as shown in Fig. 2b and d.

An electrochemical test system was used for in-situ electrochemical measurements at the fourth hour of the FAC tests. A three-electrode electrochemical cell was constructed in test section with the array electrodes as working electrodes (WE), a platinum plate as counter electrode (CE) and a saturated calomel electrode (SCE) as reference electrode (RE). To determine the inhibition efficiency of each array electrode, electrochemical impedance spectroscopy (EIS) measurements were performed at open circuit potential with an amplitude of 10 mV and the frequency from 10,000 Hz to 0.1 Hz. Then, the inhibition efficiency ($\eta\%$) was determined by the charge transfer resistance according to equation (1). To study the inhibitive mechanism of inhibitor, EIS measurements were also performed on some representative array electrodes with the frequency from 100,000 Hz to 0.01 Hz. FAC tests were performed with flow velocity of 0, 2 m/s and 4 m/s, TAI concentrations of 0, 1 ppm, 10 ppm, 50 ppm, 100 ppm and 200 ppm, 60 °C and atmospheric pressure. The FAC tests lasted 5 h.
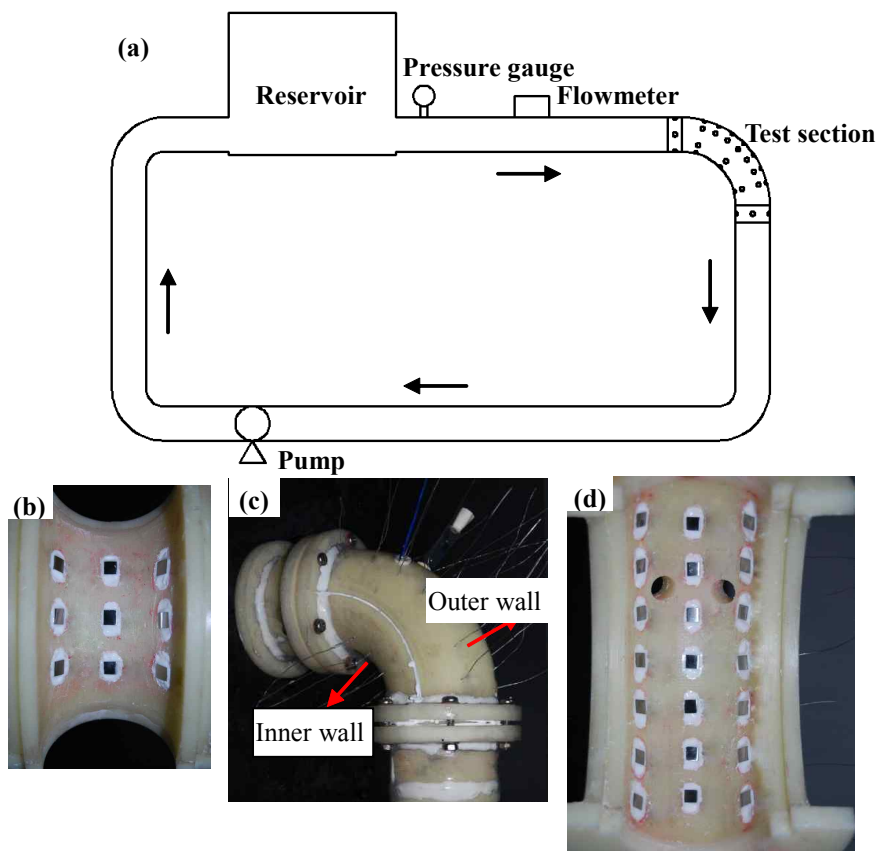

Fig. 2 Schematic diagram of the loop system and array electrodes for FAC test: (a) loop system, (b) array electrodes at the inner wall, (c) assembly of the elbow test section, and (d) array electrodes at the outer wall.
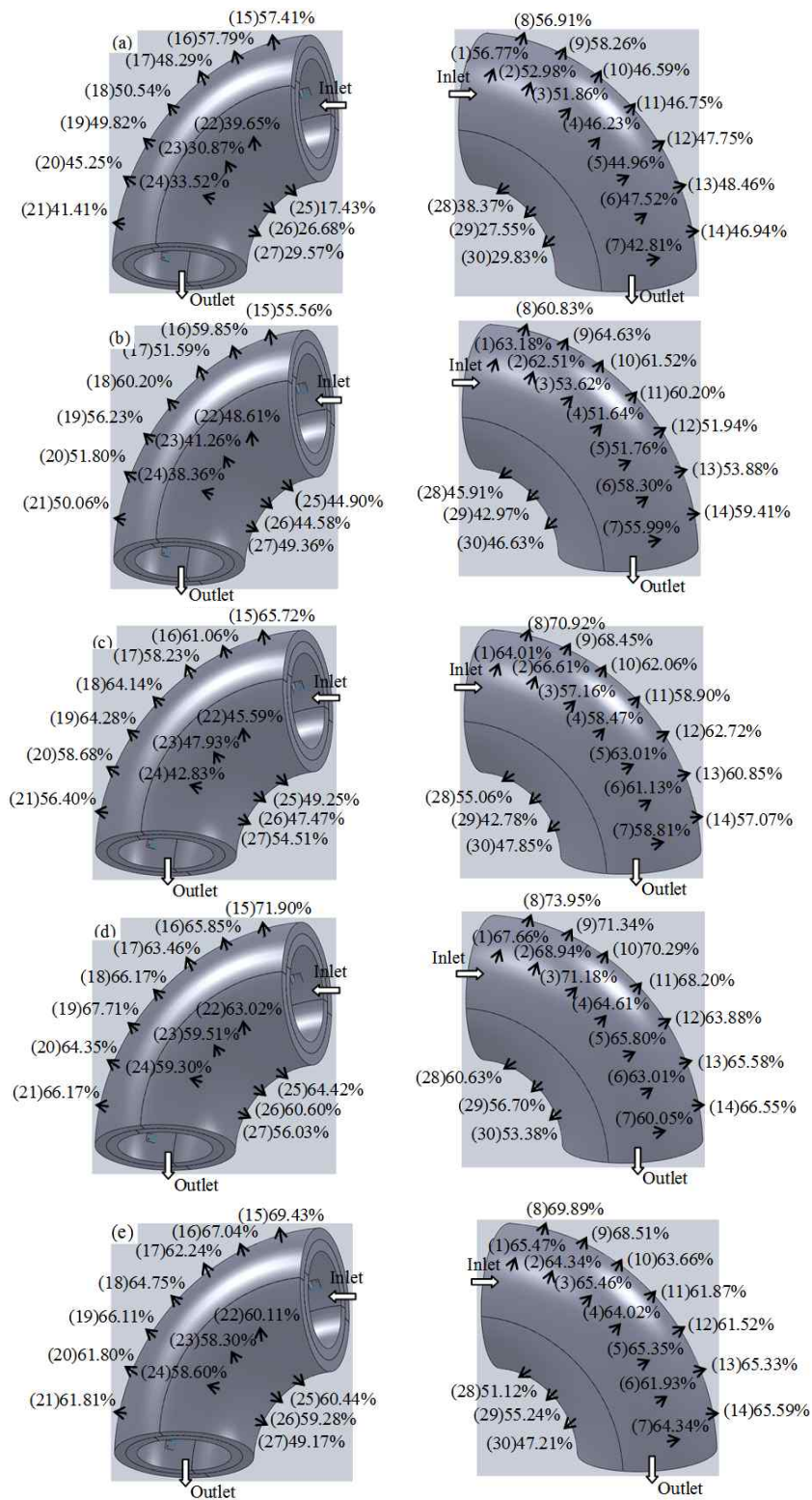
Fig. 3 Distribution of the inhibition efficiency of TAI at the elbow with different concentrations at 4 m/s: (a) 1 ppm, (b) 10 ppm, (c) 50 ppm, (d) 100 ppm, and (e) 200 ppm.
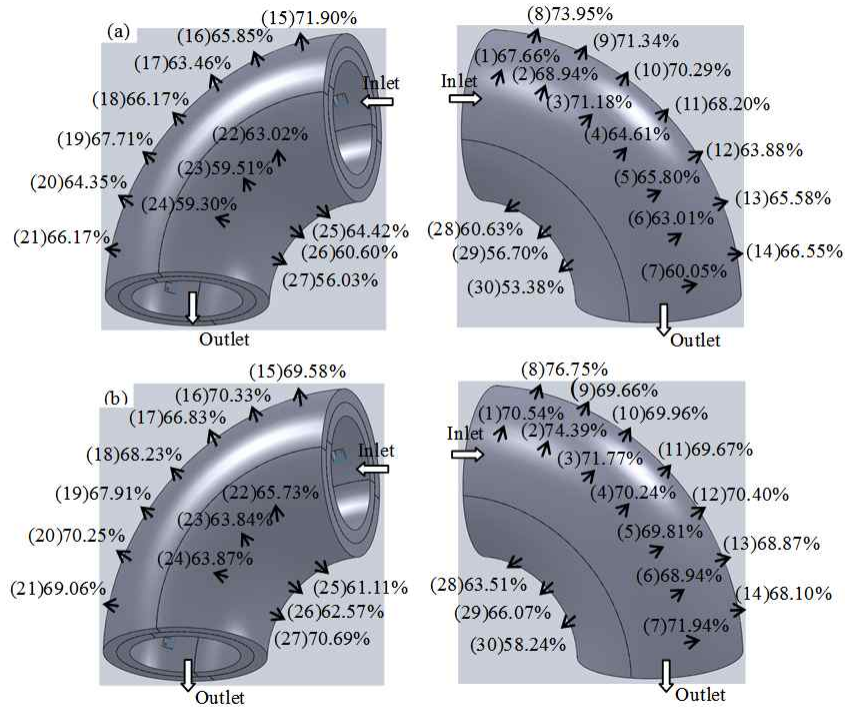
Fig. 4 Distribution of inhibition efficiency of array electrodes at the elbow test section at different flow velocities with 100 ppm inhibitor: (a) 4 m/s, and (b) 2 m/s.

$$\eta\% = \frac{R_{ct} - R_{ct}^0}{R_{ct}} \times 100 \qquad (1)$$

where R_{ct} is the charge transfer resistance with inhibitor, and R_{ct}^0 is the charge transfer resistance without inhibitor.

After FAC tests, the surface morphologies of array electrodes were observed by scanning electron microscope (SEM).

CFD simulation was performed by software Fluent. The interval size of meshes is 0.004 m. A flow velocity of 4 m/s at the inlet and outflow at the outlet were the boundary conditions. A κ-ε turbulent model was used to solve the simulation as Reynolds number is 199043. Turbulent kinetic energy κ, turbulent dissipation rate ε, turbulence intensity was set as 1 m²/s², 1 m²/s³, 3.5%, respectively. Wall roughness was set as 10 μm. Convergence criterion was up to 1×10^{-10}.

3. Results

Fig. 3 shows the distribution of the inhibition efficiency of TAI at the elbow with different concentrations at 4 m/s.

Compared to an inhibition efficiency of 95.3% at static condition with 100 ppm TAI, the inhibition efficiency for FAC is relatively low in all the different TAI concentrations. These low inhibition efficiencies should be due to drastic turbulence flow and high wall shear stress during the FAC test, which prevents the adsorption of inhibitor and/or damages the adsorbed inhibitor film. The inhibition effect of TAI at the same location of the elbow with different concentrations exhibits a peak-value-phenomenon of inhibitor concentration, i.e., there exists an optimum concentration (100 ppm) where the lowest corrosion rate and highest inhibition efficiency are present. The inhibition efficiency increases from 1ppm to 100 ppm, but decreases from 100 ppm to 200 ppm. This situation could be associated with the adsorption mode of inhibitor. This peak-value-phenomenon of inhibitor concentration was also verified by other researchers [9,10]. When the inhibitor concentration is lower than 100 ppm, the inhibitor molecules adsorb on the active sites parallel to the electrode surface including the long hydrocarbon chain. In this case, the higher inhibitor concentration means more inhibitor molecules adsorbed on the electrode surface, and then the more active sites being blocked. Therefore, inhibition efficiency increases up to the concentration of 100 ppm. When inhibitor concentration exceeds 100 ppm, the long hydrocarbon chain tends
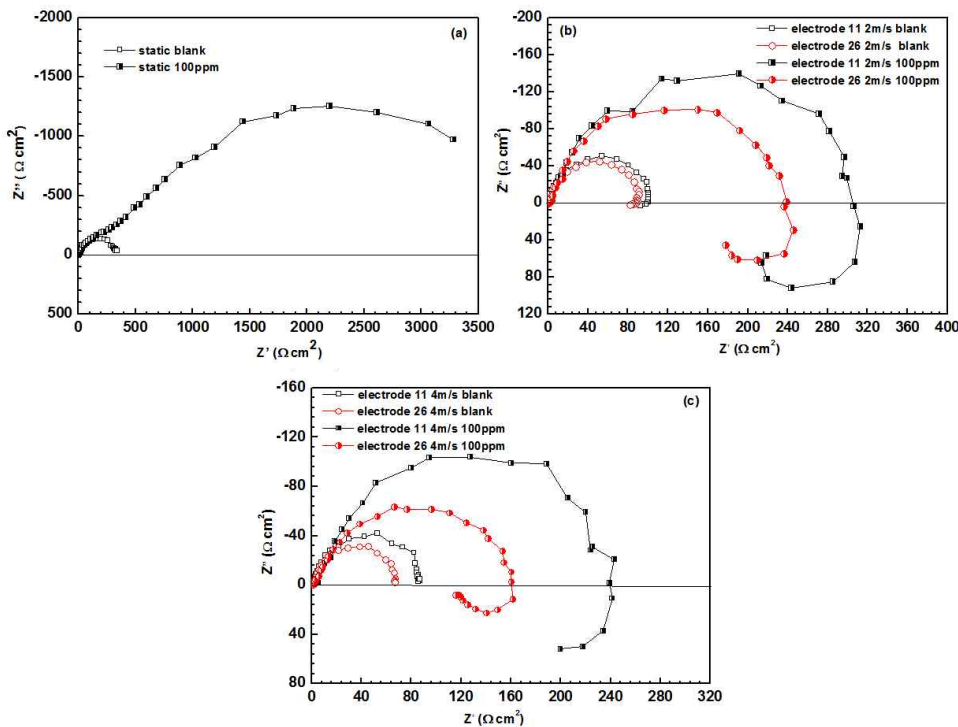
Fig. 5 Nyquist plots of representative array electrodes under FAC conditions after 4h exposure at different flow velocities: (a) static, (b) 2 m/s, and (c) 4 m/s.

to perpendicularly adsorb on the electrode surface because of electrostatic repellent effect. Compared to parallel adsorption, perpendicular adsorption of inhibitor on the electrode surface would occupy a smaller surface area even in higher concentration, which results in a decrease in inhibition efficiency.

Fig. 4 shows the distribution of the inhibition efficiency of TAI at the elbow at different flow velocities with 100 ppm inhibitor. The inhibition efficiency of TAI at the same location of the elbow increases with the decrease of flow velocity.

Fig. 5 shows the Nyquist plots (at the frequency from 100,000 Hz to 0.01 Hz) of representative array electrodes (electrode 11 at the outermost side and 26 at the innermost side) with different flow velocities. It is seen that the Nyquist plots in blank solution are characterized by one capacitive loop, while the Nyquist plots in presence of inhibitor under flow condition are characterized by a capacitive loop in the high frequency range and an inductive loop in low frequency range. The capacitive loop should be attributed to the interfacial charge transfer process while the inductive loop should be related to the poor inhibitor film and/or corrosion products on the electrode surface. The adsorbed inhibitor film may be removed due to high wall shear stress and turbulence kinetic energy

under flow condition. The repeated adsorption and desorption of inhibitor cause the inductive effect. However, the Nyquist plot in presence of TAI in static state is characterized by double capacitive loops. Compared to the blank solution, the larger diameter of the capacitive loop with inhibitor indicates the adsorption of inhibitor on the electrode surface. Furthermore, the diameter of capacitive loop increases with decreasing the flow velocity. The diameter of capacitive loop of electrode 11 is larger than that of electrode 26 in both the blank and inhibited solutions.

Fig. 6 shows the SEM surface morphologies of representative array electrodes 11 and 26 after FAC test at 4 m/s. It is seen that all the electrodes in blank and inhibited solutions are covered by corrosion products, indicating the poor inhibition effect of inhibitor at such a high flow velocity. In the absence of inhibitor, loose corrosion products are observed on the electrode surface, as shown in Fig. 6a and c. While the surface morphologies in the presence of 100 ppm inhibitor are characteristic of thin and compact corrosion products, which indicates that the inhibitor is effective under the flow condition. Furthermore, the corrosion products are more compact at the outer wall (electrode 11) than those at the inner wall (electrode 26) of the elbow with inhibitor.
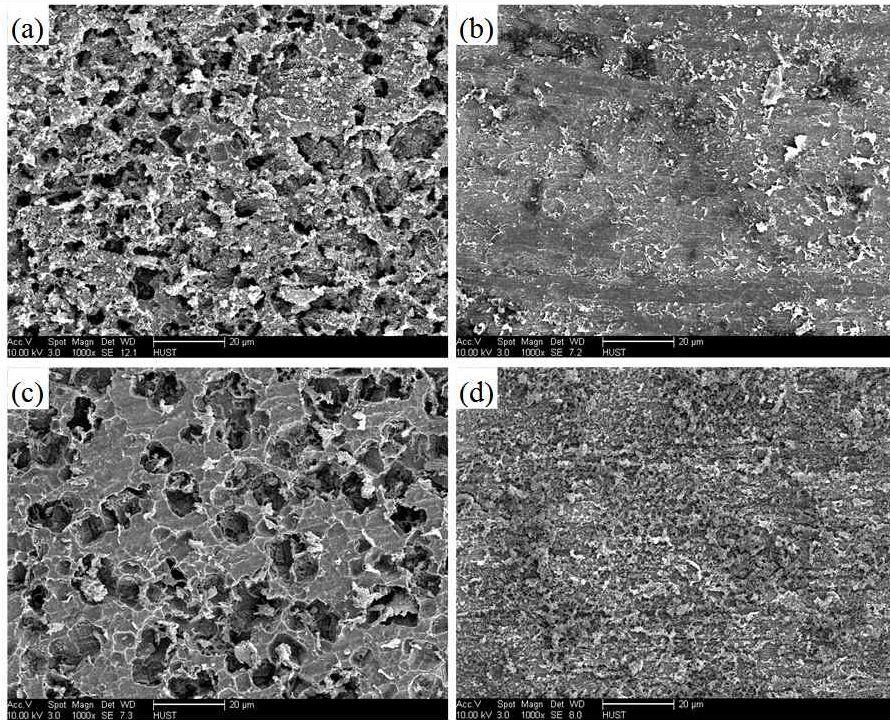
Fig. 6 SEM surface morphologies of electrodes 11 and 26 without and with 100 ppm inhibitor at 4 m/s: (a) blank for electrode 11, (b) 100 ppm inhibitor for electrode 11, (c) blank for electrode 26, and (d) 100 ppm inhibitor for electrode 26.

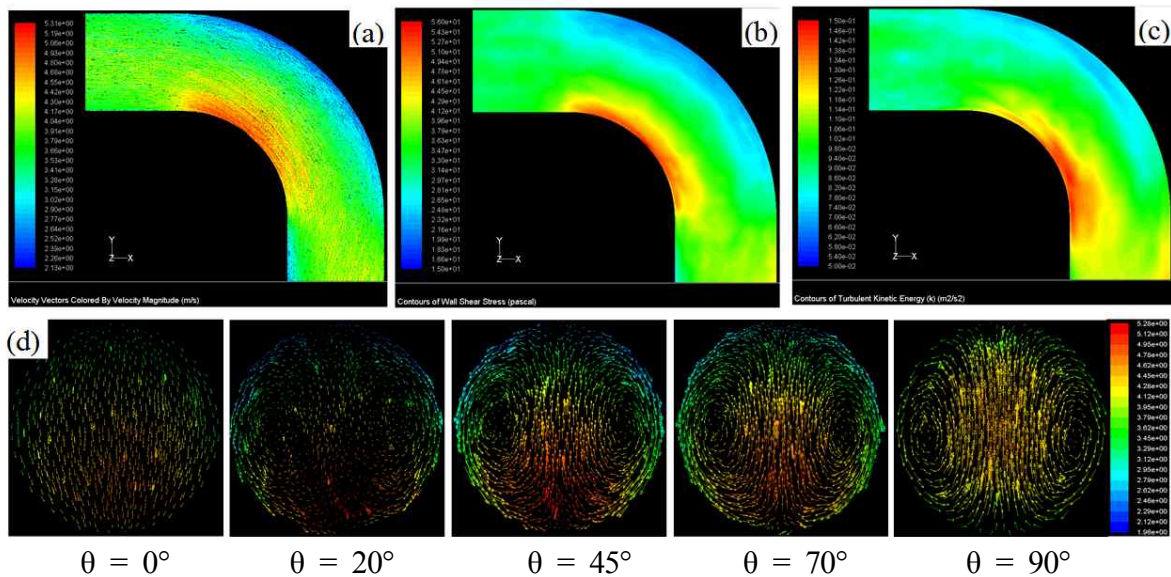| θ = 0° | θ = 20° | θ = 45° | θ = 70° | θ = 90° |

Fig. 7 CFD simulation in a 90° elbow at 4 m/s: (a) three-dimensional vectors of velocity, (b) three-dimensional contours of wall shear stress, (c) three-dimensional contours of turbulent kinetic energy, and (d) secondary flow in cross-section along the elbow.

Fig. 7 shows the three-dimensional distribution of fluid flow velocity, shear stress, turbulent kinetic energy at the elbow, and secondary flow in cross-section along the elbow with an inlet fluid flow velocity of 4 m/s. It is seen that there is similar distribution of the former three hydro-

dynamic parameters at the elbow. These hydrodynamic parameters are generally higher at the inner wall than at the outer wall. The maximum appears at the innermost side (electrode 26) while the minimum appears the outermost side (electrode 11). The secondary flow, which leads

to the formation of vortices at inner wall of the elbow [11], initiates at $\theta = 20°$, strengthens at $\theta = 45°$ and $70°$, and decays at $\theta = 90°$.

4. Discussion

The CFD simulation indicates that flow velocity, shear stress, and turbulent kinetic energy are generally higher at the inner wall than those at the outer wall. The distribution of inhibition efficiency by EIS measurements indicates that there are different inhibition effects of TAI at different locations of the elbow. Apparently, fluid hydrodynamics play an important role in the inhibition effect of TAI for the FAC at the elbow.

TAI can adsorb on the electrode surface via chemisorption mechanism involving the share of electrons between the nitrogen and iron atoms. The N=C–N bond in TAI molecule has $p-\pi$ conjugation property. In this conjugation system, π–electron is easily transferred to the d–unoccupied–orbital of Fe atom, which strengthens the chemical adsorption of N atom on the electrode surface. Adsorption can also occur in the cationic form with the positively charged part of the inhibitor molecule (ammonium–NH_3^+) oriented toward the negatively charged electrode surface as chloride ions could adsorb on electrode surface. Although coulombic attraction between the negative charge and TAI is not a primary contributor to the adsorption of TAI, it may also contribute to the inhibition ability of TAI.

The adsorption of TAI on the electrode surface involves the replacement of the adsorbed water molecules by inhibitor molecules. Then the adsorbed inhibitor will combine with the dissolved Fe^{2+} ions to form Fe-inhibitor complex [12,13]. Therefore, there are different effects of fluid flow on the inhibition performance of TAI under flow condition. On one hand, flow of fluid promotes the mass transport of inhibitor molecules, which facilitates inhibitor molecules to reach the electrode surface. On the other hand, hydrodynamic conditions with the high shear stress and turbulence kinetic energy will remove the adsorbed $[Fe–Inh]^{2+}$ complex, resulting in a low inhibitor efficiency. The balance of these effects leads to the difference in the inhibition effect of TAI at different locations of the elbow.

Apparently, in present work, the harmful effect of hydrodynamics dominates the inhibitor performance during the FAC process. At the inner wall of the elbow, the high flow velocity, and thus the high mass transfer rate, will enhance the transportation of the dissolved Fe^{2+} ions from the electrode surface to bulk solution, then slowing down the formation of $[Fe–Inh]^{2+}$ complex on the electrode

surface. Moreover, under the impingement of the fluid with a high wall shear stress and turbulence, the adsorbed inhibitor film would be removed continuously from the electrode surface. Furthermore, the second flow (Fig. 7d), which is the characteristic flow at the elbow due to its curvature, leads to the formation of vortices at the inner wall of the elbow. These vortices would also disturb the adsorption of inhibitor and damage the adsorbed inhibitor film and corrosion products on the steel surface [14]. The SEM morphologies (Fig. 6) indicate a less complete and compact corrosion product film on the electrode surface at the inner wall of the elbow. Therefore, it is obvious that the inhibition efficiencies of TAI at different locations of elbow are in good agreement with the distributions of hydrodynamic parameters.

The inhibition efficiency with different velocities shows that inhibition efficiency decreases with the increase of flow velocity. For the turbulence flow in the pipelines, the Sherwood number can be calculated by Reynolds number and Schmidt number [15]:

$$Sh = 0.0165\,Re^{0.86}\,Sc^{0.33} \qquad (2)$$

where Sh is the Sherwood number (Sh = Kd/D), Re is the Reynolds number (Re = Vd/v), Sc is the Schmidt number (Sc =v/D), d is the pipe diameter. V is the flow velocity, v is kinematic viscosity. Then the mass transfer coefficient K at the elbow can be thus obtained:

$$K = 0.0165V^{0.86}d^{-0.14}v^{-0.53}D^{0.67} \qquad (3)$$

As the flow velocity increases, the mass transfer process will be accelerated. The higher turbulence with an increasing velocity restrains the $[Fe–Inh]^{2+}$ complex from adsorbing on the surface, and higher wall shear stress damages the inhibitor film formed on the electrode. Thus, the effect of inhibitor is degraded to a lower level with the increase of flow velocity.

5. Conclusions

A novel method by combining array electrode technique with CFD simulation is proposed to determine the correlation between the inhibition effect of TAI at the elbow of pipeline and the hydrodynamics of the fluid. It is demonstrated that the inhibition efficiencies of TAI at the inner wall of the elbow are lower than those at the outer wall of the elbow, which is associated with the higher flow velocity, wall shear stress, and turbulent kinetic energy at the inner wall, as well as secondary flow at the elbow.

The inhibition efficiencies of TAI at different locations of the elbow are in good agreement with the distribution of hydrodynamic parameters.

Compared to static condition, the inhibition efficiency of TAI for FAC is relatively low. The low inhibition efficiency should be attributed to drastic turbulence flow and high wall shear stress during the FAC test, which prevents the adsorption of inhibitor and/or damages the adsorbed inhibitor film.

Acknowledgements

References

1. X. Jiang, Y. B. Zheng, and W. Ke, *Corros. Sci.*, **47**, 2636 (2005).
2. A. Neville and C. Wang, *Wear*, **267**, 2018 (2009).
3. S. Ramachandran and V. Jovancicevic, *Corrosion*, **55**, 259 (1999).
4. P. C. Okafor, X. Liu, and Y. G. Zheng, *Corros. Sci.*, **51**, 761 (2009).
5. W. Durnie and R. D. Marco, *J. Electrochem. Soc.*, **146**, 1751 (1999).
6. M. Heydari and M. Javidi, *Corros. Sci.*, **61**, 148 (2012).
7. Y. Chen and T. Hong, *Corros. Sci.*, **42**, 979 (2000).
8. M. El-Gammal, H. Mazhar, J. S. Cotton, S. Shefski, J. Pietralik, and C. Y. Ching, *Nucl. Eng. Des.*, **240**, 1589 (2010).
9. N. Hackerman, D. D. Justice, and E. McCafferty, *Corrosion*, **31**, 240 (1975).
10. I. Singh, *Corrosion*, **49**, 473 (1993).
11. B. Poulson and R. Robinson, *Int. J. Heat Mass Tran.*, **31**, 1289 (1988).
12. E. E. Oguzie, Y. Li, and F. H. Wang , *J. Colloid Interf. Sci.*, **310**, 90 (2007).
13. D. M. Ortega-Toledo, J. G. Gonzalez-Rodriguez, M. Casales, L. Martinez, and A. Martinez-Villafane, *Corros. Sci.*, **53**, 3780 (2011).
14. M. M. Enayet, M. M. Gibson, A. M. K. P. Taylor, and M. Yianneskis, *Int. J. Heat Fluid Fl.*, **3**, 213 (1982).
15. C. Deng, K. Adams, and T. MacFarlane, *Proc. NACE Corrosion Conf.*, Paper no.565, NACE International, Houston (2008).